Solid-State NMR and X-ray Studies of the Structural Evolution of Nanocrystalline Zirconia

A. V. Chadwick,[†] G. Mountjoy,[†] V. M. Nield,[†] I. J. F. Poplett,[‡] M. E. Smith,*[,‡] J. H. Strange,[†] and M. G. Tucker[†,§]

School of Physical Sciences, University of Kent, Canterbury, Kent, U.K. CT2 7NR, and Department of Physics, University of Warwick, Coventry, U.K. CV4 7AL

Received August 2, 2000. Revised Manuscript Received November 13, 2000

A combination of X-ray techniques [diffraction and Zr K-edge absorption (EXAFS and XANES)] and multinuclear (^{1}H, ^{13}C, ^{17}O) solid-state NMR spectroscopy is employed to follow in detail the structural development of nanocrystalline zirconia. ^{17}O magic-angle spinning NMR spectroscopy of sol−gel produced undoped ZrO_2 shows unequivocally that oxygen sites in the initial gel are monoclinic-like. This result is consistent with X-ray absorption measurements, which also suggest that the structures of the initial amorphous phases of doped and undoped samples produced by the hydroxide-precipitation and sol−gel methods are very similar. On crystallization, the local structure of the crystalline component is tetragonal, but a significant fraction of the sample remains disordered. Heating to higher temperatures results in conversion to monoclinic zirconia in undoped samples at room temperature. For sol−gel-produced ZrO_2, ^{13}C NMR shows that loss of all of the organic fragments occurs prior to crystallization. The ^{1}H NMR experiments determined that the proton content remains significant until well above the crystallization temperature, so that the composition is not accurately described as ZrO_2 until >500 °C.

1. Introduction

Zirconia is an extremely important material with wide-ranging applications including as a high-performance transformation-toughened structural engineering ceramic[1,2] and as a solid electrolyte[1,3] (leading to applications as an oxygen sensor[4] and as a fuel cell electrolyte[5]). Zirconia has also found application as a catalyst and catalyst support,[6,7] especially when durability to chemical attack is required. A common formation method is to begin with a soluble zirconium salt dissolved in water and to form an amorphous zirconium hydroxide precipitate by increasing the pH.[8,9] The precipitate is then calcined to form tetragonal zirconia, which, in undoped bulk zirconia, transforms to monoclinic zirconia when it is cooled back to room temperature.[1] Even this relatively simple process is difficult to fully characterize as the hydroxide intermediate is amorphous.[9] The tetragonal phase is stabilized at room temperature by dopants.[10] Many additional factors[11] have been suggested as stabilizing the tetragonal phase at room-temperature, including crystallite size,[12] impurities (e.g., OH^-, Cl^-, SO_4^-), structural similarity of the precursor amorphous phase, strain effects, and lattice defects. A comparison of the preparation of ZrO_2 using X-ray diffraction and electron microscopy from basic zirconium sulfate and zirconium oxychloride showed that crystallization and subsequent phase transformations were dependent on the preparation and suggested that crystallite size was not a determining factor in the tetragonal (t) to monoclinic (m) phase transition.[13] A more recent study of ultrafine zirconia powders prepared from $ZrOCl_2$ and zirconium *n*-butoxide showed that synthesis and processing affect crystallization and phase transitions and again suggested that the t → m phase transition was not criticially affected by the particle size.[14]

Both the hydroxide-precipitation and especially the sol−gel method[15] offer much scope for initial atomic-scale mixing of dopants and subsequent partial crystallization to form genuinely nanocrystalline materials.

* Author for correspondence: M. E.Smith, Department of Physics, University of Warwick, Coventry, U.K. CV4 7AL. E- mail: M. E.Smith.1@warwick.ac.uk.

[†] University of Kent.

[‡] University of Warwick.

[§] Current address: Department of Earth Sciences, University of Cambridge, Downing Street, Cambridge, U.K. CB2 3EQ.

(1) Stevens, R. *An Introduction to Zirconia*; Magnesium Elektron Ltd: London, 1986.

(2) Garvie, R. C.; Hannink, R. H.; Pascoe, R. T. *Nature* **1975**, *258*, 703.

(3) Steele, B. C. H. *Solid State Ionics* **1995**, *75*, 157.

(4) Steele, B. C. H.; Drennan, J.; Slotwinski, R. K.; Bonanos, N.; Butler, E. P. *Advances in Ceramics*; Heuer, A. H., Hobbs, L. W., Eds.; American Ceramic Society: Columbus, OH, 1981; Vol. 3, p 286.

(5) Badwal, S. P. S. *Appl. Phys. A* **1990**, *50*, 449.

(6) Tanake, K.; Yamaguchi, T. *Catal. Today* **1994**, *20*, 185.

(7) Davis, B. H.; Keogh R. A.; Srinivasan, R. *Catal. Today* **1994**, *20*, 219.

(8) Clearfield, A. *Rev. Pure Appl. Chem.* **1964**, *14*, 91.

(9) Turrillas, X.; Barnes, P.; Gascoigne, D.; Turner, J. Z.; Jones, S. L.; Norman, C. J.; Pygall, C. G.; Dent, A. J. *Radiat. Phys. Chem.* **1995**, *45*, 491.

(10) Subbarao, E. C. *Ferroelectrics* **1990**, *102*, 267.

(11) Wu, F. C.; Yu, S. C. *J. Mater. Sci.* **1990**, *25*, 970.

(12) Garvie, R. C. *J. Phys. Chem.* **1978**, *82*, 218.

(13) Bernstein, E.; Blanchin, M. G.; Ravelle-Chapuis, R.; Rodriguez-Carvajal, J. *J. Mater. Sci.* **1992**, *27*, 6519.

(14) Hu, M. Z. C.; Hunt, R. D.; Payzant, E. A.; Hubbard, C. R. *J. Am. Ceram. Soc.* **1999**, *82*, 2313.

(15) Brinker, C. J.; Scherer, G. W. *Sol−Gel Science*; Academic Press: San Diego, CA, 1990.

10.1021/cm001152w CCC: $20.00
Published on Web 03/09/2001

Nanocrystalline materials have engendered much research interest over the past decade as such samples offer significant changes in both the bulk properties (e.g., enhanced plasticity of TiO_2[16]) and the catalytic activity.[17] In catalytic applications, the possible advantages of such materials include increased surface area, distinct surface morphologies that can be advantageously different from the bulk forms, and the ability to dissolve higher concentrations of impurities.[18,19] Samples made up of small particles of partially crystallized ZrO_2 are probably complex mixtures of tetragonal, monoclinic, and amorphous regions, with also the possibility of some cubic and orthorhombic components.[20] Obtaining a thorough understanding of such materials by applying a characterization methodology that can follow in detail the structural evolution in such particles is a challenge.

In this study, a synchrotron is used to provide an intense X-ray source to allow in situ diffraction to be combined with atomic-scale information from zirconium K-edge EXAFS (extended X-ray absorption edge fine structure) and XANES (X-ray absorption near edge structure) spectrocopies. Detailed studies of zirconia have been previously carried out on bulk phases using the EXAFS technique[21,22] and on the structural development of amorphous hydroxide precursors and subsequent crystalline-phase conversion on cooling using energy-dispersive diffraction and EXAFS studies.[9] We have collected EXAFS, XANES, XRD and multinuclear (^{1}H, ^{13}C, ^{17}O) solid-state NMR data (^{91}Zr NMR has been shown to be able to distinguish the polymorphs of ZrO_2, but in the complex mixtures produced here, the resonances would strongly overlap[23]). The low natural abundance of ^{17}O (0.037%) means that isotopic enrichment is necessary for routine observation. This can be efficiently achieved in the hydrolysis step[15] of the sol−gel process and was carried out here for the undoped ZrO_2 sample. The sensitivity of the ^{17}O chemical shift has shown a wide variation in the detailed nature of the intermediate states in the sol−gel production of different oxides including TiO_2,[24] MgO,[25] and HfO_2.[26] Despite having a quadrupole moment, quadrupole effects on the central ($^1/_2$, $-^1/_2$) transition are effectively negligible in ionic oxides.

Studies of the crystallization of La_2O_3[27,28] and MgO[25] gels have shown that the combination of synchrotron and solid-state magic-angle spinning (MAS)[29] NMR techniques is extremely powerful in elucidating structural development. This current study uses in situ synchrotron techniques to examine the structural development up to crystallization of some samples and ex situ studies for samples heated over a greater temperature range. The synchrotron results compare the hydroxide-precipitation and sol−gel routes and examine the effect of yttrium doping. The extensive ^{17}O NMR data of the sol−gel-prepared undoped sample presented here considerably improves on our preliminary NMR report[30] and has allowed greatly extended data analysis. This corroborates some of the speculative structural models previously advanced.[30]

2. Method

2.1. Sample Preparation. For the hydroxide-precipitation route, 50 g of $ZrOCl_2 \cdot 8H_2O$ was dissolved in 200 mL of H_2O and stirred to give a 0.78 M solution. For doped samples, a sufficient amount of an aqueous solution of $YCl_3 \cdot 6H_2O$ was added to produce an 8 mol % yttrium content. Aqueous $NH_4(OH)$ solution was then added dropwise until the pH was increased to ∼10 as determined by Universal Indicator paper. Subsequently, a precipitate formed, and the solution was stirred for approximately another hour. The precipitate formed was suction filtered and washed several times with distilled water (to remove as much chloride as possible by washing) until the filtrate reached pH 7 to leave a clean "as-made" amorphous, hydrous zirconia. This sample was then dried at 110 °C for a couple of days.

In the sol−gel preparation, zirconium *n*-propoxide propanol complex [$Zr(OPr)_4 \cdot PrOH$] was dissolved in dry propanol in the approximate ratio 1:1. H_2O was then added dropwise to the zirconium−propanol mixture to give a water:zirconium ratio of 3:5 (i.e., an excess of water). For doped samples, yttrium was added as $Y(NO_3)_3$ dissolved in the added water. On addition of water, very rapid precipitation occurred, but the mixture was left for 24 h before being dried at 110 °C. No acid or alkali was added. For the ^{17}O sample, 46 at. % ^{17}O-enriched water was used, in the same ratio to the other components as for the other reactions. For this enriched sample the excess liquid was removed by vacuum evaporation at room temperature to leave a slightly damp "as-made" product.

Samples were heated at 5 °C/min in a tube furnace under a normal atmosphere to the target temperature, left at that temperature for ∼2 h, and then cooled rapidly back to room temperature. For the ^{17}O-enriched sample, the only differences were that the same sample was successively heated to higher temperatures and a nitrogen atmosphere was used to limit the loss of the ^{17}O isotope by exchange.

2.2. NMR Measurements. NMR spectroscopy was performed on a Chemagnetics CMX 300 spectrometer equipped with a 7.05-T magnet using a Chemagnetics double-bearing 4-mm probe. Room-temperature ^{17}O MAS NMR spectra using spinning speeds of 10−15 kHz were recorded at a frequency of 40.707 MHz using a

(16) Birringer, R.; Hahn, H.; Hoefler, H.; Karch, J.; Gleiter, H. *Defect Diffus. Forum* **1988**, *59*, 17.
(17) Henglein, A. *Chem. Rev.* **1989**, *89*, 1061.
(18) Stark, J. V.; Klabunde, K. J. *Chem. Mater.* **1996**, *8*, 1913.
(19) Koper, O.; Lagadic, I.; Klabunde, K. J. *Chem. Mater.* **1997**, *9*, 838.
(20) Wang, Y.; Lu, K.; Wang, D.; Wu, Z.; Fang, Z. *J. Phys.: Condens. Matter* **1994**, *6*, 633.
(21) Li, P.; Chen, I.-W.; Penner-Hahn, J. E. *Phys. Rev. B* **1993**, *48*, 10063.
(22) Li, P.; Chen, I.-W.; Penner-Hahn, J. E. *Phys. Rev. B* **1993**, *48*, 10074.
(23) Bastow, T. J.; Smith, M. E. *Solid State Nucl. Magn. Reson.* **1992**, *1*, 165.
(24) Bastow, T. J., Moodie, A. F.; Smith, M. E.; Whitfield, H. J. *J. Mater. Chem.* **1993**, *3*, 697.
(25) Chadwick, A. V.; Poplett, I. J. F.; Maitland, D. T. S.; Smith, M. E. *Chem. Mater.* **1998**, *10*, 864.
(26) Bastow, T. J.; Smith, M. E.; Whitfield, H. J. *J. Mater. Chem.* **1996**, *6*, 261.
(27) Ali, F.; Smith, M. E.; Steuernagel, S.; Whitfield, H. J. *J. Mater. Chem.* **1996**, *6*, 1951.
(28) Ali, F.; Chadwick, A. V.; Smith, M. E. *J. Mater. Chem.* **1997**, *7*, 285.
(29) Andrew, E. R. *Int. Rev. Phys. Chem.* **1981**, *1*, 195.
(30) Bastow, T. J.; Smith, M. E.; Whitfield, H. J. *J. Mater. Chem.* **1992**, *2*, 989.

spin−echo sequence with a ∼40-μs echo spacing and extended phase cycling,[31] with the pulses producing an rf field of ∼7 mT. A recycle delay of 1−10 s was used, sufficient to produce relaxed spectra. Additionally, some static ^{1}H−^{17}O CP spectra were recorded with the Hartmann−Hahn match condition set on ^{17}O-enriched $Mg(OH)_2$ and a contact time of 50 μs. The short contact time gave the largest signal and static spectra were used because MAS severely attenuated the CP signal. ^{13}C MAS NMR spectra were accumulated at 75.512 MHz using MAS of 5 kHz, ^{1}H−^{13}C CP spectra with a contact time of 1 ms and a recycle delay of 1 s. Some direct one-pulse ^{1}H MAS NMR spectra were accumulated using fast MAS of 15 kHz at a resonance frequency of 300.304 MHz. To allow quantification of the proton content, a ^{1}H spectrum was also collected on pure adamantane (Aldrich), and both the sample and the standard were carefully weighed. All spectra were referenced to external standards of H_2O for ^{17}O at 0 ppm, the CH_2 of adamantane for ^{13}C at 38.56 ppm and tetramethylsilane for ^{1}H at 0 ppm.

2.3. Synchrotron X-ray Experiments. *2.3.1. Combined Diffraction and EXAFS Measurements.* The powder samples were pressed into 13-mm-diameter pellets with an equal mass of sample and fumed silica powder (usually, 20 mg of each made strong pellets with good X-ray absorption). The XRD data were recorded at a wavelength of 0.7018 Å using a curved position sensitive detector. Samples were dried at 110 °C, heated to 200 °C, and then heated in successive 10 °C steps, with each temperature being held for ∼15 min and with the crystallization temperature determined as the point at which Bragg peaks first appeared. An estimate of the crystallite size (S) was obtained by applying the Scherrer equation,[32] i.e., $S = K\lambda/\beta\cos\theta$, where K is a constant (∼0.89), β is the full width at half-maximum of a diffraction peak at angle 2θ, and λ is the X-ray wavelength.

Note that, for the ^{17}O-enriched samples, the particle size was determined from XRD patterns obtained on a conventional laboratory powder diffractometer (Phillips PW1050) using Cu Kα radiation (λ = 0.1544 nm), scanning a 2θ range of 20−100° at a rate of 1° min^{-1}. The crystallization temperature was found by varying the temperature from just below the crystallization temperature determined by in situ synchrotron studies in 10 °C steps with each temperature held for ∼2 h.

Combined transmission quick EXAFS of the Zr K-edge and XRD studies were carried out on Station 9.3 at the CCLRC Daresbury Laboratory SRS, U.K.[33] EXAFS data were collected using a double silicon (220) crystal monochromator that was detuned at ∼65% of the maximum to reject higher-order harmonics. The energy scale was calibrated using the point of inflection of the main absorption edge of a zirconium foil at 17998 eV (E_o). The absorbance (μ) was measured in standard transmission mode using ion chambers before and after the sample, with the thickness of the sample producing an absorption edge jump of ∼1. The EXAFS spectrum is given by $\chi(k) = [\mu(k) - \mu_{post}(k)]/[\mu_{pre}(k) - \mu_{post}(k)]$, where $\mu_{pre}(k)$ and $\mu_{post}(k)$ are fits to the pre- and postedge backgrounds, respectively. Typical collection times were 720 s for the EXAFS measurements over an energy range of ∼30−643 eV, and 180 s for the XRD measurements.

In single-scattering curved wave theory, the absorption $\chi(k)$ at wavevector k has the form[34]

$$\chi(k) = S_0^2(k) \sum_j \frac{N_j}{kR_j^2} |f(k,R_j)| e^{-R_j/\lambda(k)} e^{-2\sigma_j^2 k^2} \times \sin[2kR_j + 2\delta(k) + \phi(k,R_j)] \quad (1)$$

where $S_0^2(k)$ is the amplitude reduction factor from multielectron effects, N_j is the number of atoms at a distance R_j from the central absorbing atom, and $2\sigma_j^2$ is the Debye−Waller (DW) factor taking into account the structural and thermal disorder. Other parameters are the phase shifts due to the central excited atom [$\delta(k)$] and the backscattering atom [$\varphi(k,R_j)$], the backscattering amplitude, [$|f_j(k,R_j)|$], and the inelastic mean free path of the photoelectron, [$\lambda(k)$].

No window function was used for the EXAFS data, which were conventionally processed using the Daresbury suite of programs EXCALIB, EXBACK, and EXCURV92.[35,36] Data were fitted from ∼3.5 Å^{-1} up to 13 Å^{-1} with k^3 weighting. $S_0^2(k)$ was varied in the initial fitting of the model compounds and was found to remain close to 0.8; thus, it was fixed at 0.8 in all further refinements. A series of simulations was carried out with the coordination numbers fixed at values corresponding to those of the bulk phases. Fixing the coordination number at reasonable integer values has been adopted in previous EXAFS studies of zirconia.[21] This philosophy means that R_j and $2\sigma_j^2$ are iterated to minimize the fit index given by $\sum_i[k^3(\chi_i^T - \chi_i^E)]^2$. Choosing the coordination numbers means that the EXAFS results produce a structure closely related to that of the starting crystalline phase. Simulations were tried starting from the parameters for each of the crystalline forms, so this approach indicates which of these structures most closely resembles the amorphous state. As R_j and $2\sigma_j^2$ are varied, the errors in these values indicate the quality of each structure at simulating the data. The data could also be simulated by combining shells from different structures to give a mixture of structures, but there is insufficient resolved detail in the experimental data to allow the ambiguity of different simulations to be accurately judged.

As the pairs of parameters R_j and E_f (a correction of the energy E_o) and N_j and $2\sigma_j^2$ are highly correlated,[37] the statistical errors were estimated from the 95% confidence level as a function of the fitted parameters in the respective pairs. Statistical errors will underes-

(31) Kunwar, A. C.; Turner, G. L.; Oldifield, E. *J. Magn. Reson.* **1986**, *69*, 124.
(32) King, H. P.; Alexander, L. E. *X-ray Procedures*; Wiley: New York, 1974.
(33) Sankar, G.; Wright, P. A.; Natarajan, S.; Thomas, J. M.; Greaves, G. N.; Dent, A. J.; Dobson, B. R.; Ramsdale, C. A.; Jones, R. H. *J. Phys. Chem.* **1993**, *97*, 9550.
(34) Mustre de Leon, J.; Zabinsky, S. I.; Albers, R. C. *Phys. Rev. B* **1995**, *52*, 2995.
(35) Dent, A. J., Mosselmans, J. F. W. *Guides to EXCALIB, EXBACK and EXCURV92*; Daresbury Laboratory: Cheshire, U.K., 1995.
(36) Binsted, N.; Campbell, J. W.; Gurman, S. J.; Stephenson, P. C. *CCLRC Daresbury Laboratory EXCURV92 Program*; Daresbury Laboratory: Cheshire, U.K., 1991.
(37) Joyner, R. W.; Martin, K. J.; Meehan, P. *J. Phys. C* **1987**, *20*, 4005.

timate the uncertainty in the results when there are also systematic errors present. The best fit was then Fourier transformed with a phase correction using the first (O) shell phase shift so that precise radial distances cannot be read off the Fourier transforms for the other shells. For in situ measurements, the as-made products were heated directly in a furnace with Kapton windows under nitrogen on the synchrotron beamline.[38]

2.3.2. XANES Measurements. The XANES experiments were performed on station 9.3 using the same conditions as described above with steps of 1.7 eV in the region from −15 to +30 eV relative to the Zr K-edge. Lifetime broadening of ∼2 eV occurs at the Zr K-edge.[39] XANES spectra are given by the normalized absorption where the zero of the energy scale was determined from the point of inflection of the main absorption edge E_0. K-edge XANES measurements involve excitation of the 1s photoelectron into low-lying empty states at the central atom with p-type symmetry.[40] Preedge peaks correspond to 1s → *n*d transitions with p−d mixing. Such transitions are not allowed for completely centrosymmetric sites, but as the symmetry decreases, the intensity of such peaks increases. A fingerprinting approach is used by comparing the peak shape and position in unknown compounds with those from materials with well-defined local structures.[41]

3. Results

In situ XRD measurements showed crystallization in all samples at ∼(340 ± 10) °C [except for the undoped precipitate sample, which crystallized at ∼(320 ± 10) °C]. At the crystallization temperature, the mean crystallite size is ∼10 nm, except for the 8 mol % yttrium-containing precipitate sample, whose crystallites grew to around 15 nm. The crystallite size was also determined by XRD for samples heated to other temperatures (Table 1). Detailed in situ neutron diffraction data shows that at higher temperatures (≥500 °C), crystallization and crystallite growth in these samples become much more rapid with a quasi-equilibrium typically achieved within 2 h.[42] The crystallite size reached within 2 h increases with temperature. The phase at high temperature and in undoped ZrO_2 samples will be tetragonal, but the tetragonal-to-monoclinic conversion occurs as the sample is cooled to room temperature.[1] Apart from the in situ studies, data are reported on room-temperature samples, so that phases formed during cooling might not be the phases produced at high temperature.

EXAFS spectra were recorded from commercially produced well-defined bulk single-phase zirconia samples of monoclinic (m) (pure ZrO_2, Magnesium Elektron), tetragonal (t) (3 mol % Y_2O_3-stabilized, Tosoh Corporation, Japan), and cubic (c) (8 mol % Y_2O_3-stabilized, Tosoh Corporation, Japan) structures. The crystallographic data for starting the fitting procedure were taken from Table 1 of Li et al.,[21] and the results obtained from fitting the EXAFS data from the model compounds (Table 2) are in very good agreement with those of Li et al. For the amorphous samples, the programs were allowed to iterate starting from both the model tetragonal and monoclinic structures, with the best resulting fits given in Table 1. In all samples, starting from either the hydroxide or the sol−gel and independent of doping, similar patterns of structural development occur. In the amorphous samples, there is a well-defined (as deduced from the relatively low Debye−Waller factor) oxygen shell with a coordination number of 7 at ∼2.14 Å and a second shell with a much smaller coordination number at ∼3.42 Å corresponding to the Zr−Zr correlation. (Figure 1 shows this for the pure precipitation-produced sample.) At the crystallization temperature, there is a distinct change (Figure 1), with the oxygen correlation now better fit by two closely spaced shells and a large increase in the coordination number associated with the Zr−Zr correlation (Table 1). As the heat treatment increases, the DW factor of the Zr−Zr correlation decreases (Table 1), making it much more prominent (Figure 1). In the doped samples heated to 1000 °C, the data are very close to those for the pure bulk tetragonal phase. In the undoped samples, the EXAFS data suggest that the local structure is monoclinic at room temperature in samples that have been heated to ≥700 °C.

Zr K-edge XANES results are shown for various stages of preparation of undoped nanocrystalline ZrO_2 from the sol−gel and precipitation methods (Figure 2). For comparison, the XANES spectra from bulk m- and t-ZrO_2 are also shown. In both samples prior to crystallization, the XANES spectra more closely resemble monoclinic rather than ZrO_2. At the crystallization temperature, the XANES spectra have changed to indicate a more tetragonal structure, which persists in samples heated to 500 °C.

The center bands of the ^{17}O MAS NMR data (Figure 3) are initially characterized by two well-resolved peaks that start off at ∼400 and ∼300 ppm. As the heat treatment increases, the peak positions become more positive. This change is more noticeable for the 300 ppm peak, which moves from 303 ppm initially to 321 ppm as crystallization occurs. These spectra were simulated by using Gaussian line shapes, which show that there is a significant increase in line width initially (Table 3). At the point of crystallization (Figure 3e), an additional intermediate peak appears at ∼374 ppm corresponding to t-ZrO_2. The temperature determined in the laboratory for crystallization was (360 ± 10) °C, in reasonable agreement with the in situ synchrotron measurements of (340 ± 10) °C. XRD shows only small Bragg peaks of t-ZrO_2 (data not shown) in agreement with the crystalline phase identified by NMR results. By NMR spectroscopy, crystallization was determined by the appearance of significantly narrower (∼100%) resonances. However, the ^{17}O NMR data clearly indicate that much of the sample remains disordered. This result is in agreement with XRD data for *this* sample, which show relatively weak peaks from t-ZrO_2 and still relatively strong diffuse scattering from the amorphous component. The diffraction peaks of t-ZrO_2 increase in intensity after the sample is heated to 380 °C, and the peak at 377 ppm in the ^{17}O MAS NMR spectrum is much stronger. After sample is heated to 500 °C, this

(38) Dent, A. J.; Oversluizen, M.; Greaves, G. N.; Roberts, M. A.; Sankar, G.; Catlow, C. R. A.; Thomas, J. M. *Physica B* **1995**, *208−209*, 253.
(39) Teo, B. K. *EXAFS: Basic Principles and Data Analysis*; Springer-Verlag: Berlin, Germany, 1986.
(40) Grunes, L. A. *Phys. Rev. B* **1983**, *27*, 2111.
(41) Brydson, R.; Garvie, L. A. J.; Craven, A. J.; Sauer, H.; Hofer, F.; Cressey, G. *J. Phys.: Condens. Matter* **1993**, *5*, 9379.
(42) Nield, V. M.; Smith, M. E.; Tucker, M. G. Unpublished data.

Table 1. Summary of Synchrotron X-ray Diffraction and EXAFS from Doped and Undoped ZrO_2 Samples Produced via Precipitation and Sol−Gel Routes

		precipitation samples EXAFS								sol−gel samples EXAFS							
		pure				8% Y				pure				8% Y			
temp (°C)	shell[b]	d (Å ± 0.01)	$2\sigma^2$ (Å^2 ± 0.001)	N	phase & crystallite size from XRD[c]	d (Å ± 0.01)	$2\sigma^2$ (Å^2 ± 0.001)	N	phase & crystallite size from XRD[c]	d (Å ± 0.01)	$2\sigma^2$ (Å^2 ± 0.001)	N	phase & crystallite size from XRD[c]	d (Å ± 0.01)	$2\sigma^2$ (Å^2 ± 0.001)	N	phase & crystallite size from XRD[c]
110	Zr−O	2.14	0.017	7	amorphous	2.13	0.017	7	amorphous	2.14	0.016	7	amorphous	2.13	0.016	7	amorphous
	Zr−O																
	Zr−Zr	3.42	0.028	4		3.42	0.027	4		3.42	0.024	4		3.42	0.024	4	
250[a]	Zr−O	2.12	0.024	7	amorphous	2.11	0.025	7	amorphous	2.13	0.025	7	amorphous	2.11	0.024	7	amorphous
	Zr−O																
	Zr−Zr	3.37	0.029	4		3.36	0.033	4		3.37	0.029	4		3.37	0.028	4	
300	Zr−O	2.13	0.020	7	amorphous					2.13	0.017	7	amorphous				
	Zr−O																
	Zr−Zr	3.37	0.026	4						3.37	0.026	4					
Xtal	Zr−O	2.10	0.010	4	tetragonal	†2.11	0.014	4	tetragonal	†2.09	0.014	4	tetragonal	†2.08	0.010	4	tetragonal
temp	Zr−O	2.31	0.033	4	10 ± 1 nm	2.31	0.040	4	15 ± 1 nm	2.27	0.036	4	9 ± 1 nm	2.28	0.018	4	10 ± 1 nm
	Zr−Zr	3.61	0.025	12		3.66	0.067	12		3.62	0.044	12		3.60	0.057	12	
400	Zr−O	2.09	0.010	4	tetragonal	2.11	0.013	4	tetragonal	2.10	0.008	4	tetragonal	2.11	0.009	4	tetragonal
	Zr−O	2.30	0.031	4	12 ± 1 nm	2.31	0.040	4	15 ± 1 nm	2.30	0.027	4	9 ± 1 nm	2.28	0.027	4	10 ± 1 nm
	Zr−Zr	3.60	0.019	12		3.60	0.024	12		3.61	0.019	12		3.59	0.023	12	
500	Zr−O	2.10	0.009	4	tetragonal	2.10	0.013	4	tetragonal	2.08	0.008	4	tetragonal	2.10	0.009	4	tetragonal
	Zr−O	2.31	0.028	4	12 ± 1 nm	2.32	0.036	4	15 ± 1 nm	2.29	0.031	4	10 ± 1 nm	2.27	0.020	4	10 ± 1 nm
	Zr−Zr	3.62	0.021	12		3.60	0.020	12		3.60	0.017	12		3.59	0.020	12	
700	Zr−O	2.13	0.021	7	monoclinic/	2.10	0.009	4	tetragonal	2.10	0.009	4	tetragonal/				t
	Zr-X	3.44	0.016	7	tetragonal	2.31	0.028	4	21 ± 2 nm	2.31	0.027	4	monoclinic				
	Zr−Zr	3.96	0.018	4	25 ± 3 nm	3.62	0.017	12		3.62	0.020	12	13 ± 1 nm				
1000	Zr−O	2.14	0.023	7	monoclinic	2.10	0.012	4	tetragonal	2.12	0.020	7	monoclinic	2.10	0.009	4	tetragonal
	Zr-X	3.44	0.014	7	41 ± 10 nm	2.32	0.033	4	25 ± 3 nm	3.43	0.015	7	37 ± 8 nm	2.29	0.023	4	21 ± 2 nm
	Zr−Zr	3.97	0.016	4		3.61	0.018	12		3.91	0.017	4		3.61	0.017	12	

[a] Data were collected in situ at the temperature stated rather than heating and cooling back down to room temperature. [b] Zr−X, X = O/Zr in the dominant phase shown by XRD is tetragonal/monoclinic, respectively. [c] For the diffraction data, phase 1/phase 2 means that there is evidence for both phases but that phase 1 is dominant.

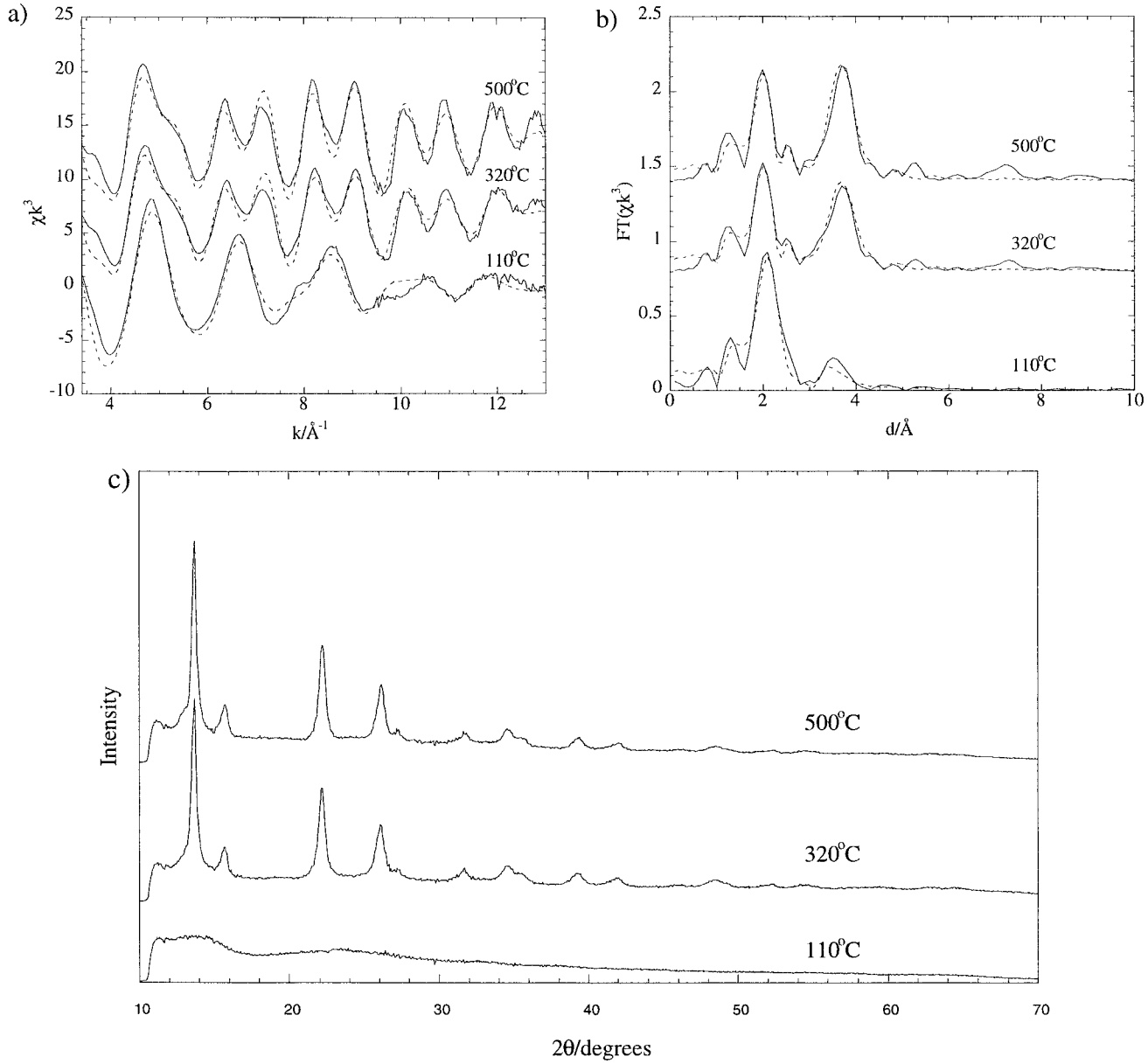

Figure 1. (a) EXAFS data; (b) corresponding Fourier transform (solid lines), along with the theoretical fits (dashed lines); and (c) XRD patterns for undoped ZrO_2 produced via the hydroxide-precipitation route after the samples were heated for 2 h at three temperatures (vertical offsets have been used for clarity.)

Table 2. EXAFS Data from Model Bulk Crystalline ZrO_2 Polymorphs

phase	correlation	bond length (Å) (± 0.01)	Debye−Waller factor ($2\sigma^2$, Å^2) (± 0.001)	coordination number (N)
monoclinic	Zr−O	2.14	0.018	7
	Zr−Zr	3.45	0.013	7
	Zr−Zr	3.99	0.017	4
tetragonal	Zr−O	2.10	0.010	4
	Zr−O	2.32	0.013	4
	Zr−Zr	3.62	0.017	12
cubic	Zr−O	2.14	0.018	7
	Zr−Zr	3.59	0.020	12

peak is dominant, but two other narrow ^{17}O resonances (at 403 and 326 ppm, corresponding to m-ZrO_2) have significant intensity, and all three have narrowed considerably (Table 3). This narrowing continues at 700 °C, but at that point, the two outer peaks are dominant and have equal integrated intensity.

Spinning sidebands can be seen for ^{17}O to extend over a range of <5000 ppm (Figure 4a), and in the sample heated to 110 °C, there is an additional peak at ∼100 ppm (Figure 4b). Using $^1H-^{17}O$ CP on this sample (Figure 4c) generates a very strong static NMR signal centered at ∼100 ppm. The 100 ppm peak is likely to arise from Zr−OH with the line broadening largely determined by the quadrupole interaction. For samples heated to 360 °C, the 100 ppm peak is not obvious in direct one-pulse experiments but is revealed by CP, albeit much weaker than in the sample heated to 110 °C.

MAS easily removes the line broadening of the protons in these samples, where there is no strong homonuclear dipolar coupling. The ^1H MAS NMR spectrum has at least four peaks at 4.9, 2.7, 0.7, and 0 ppm (Figure 5a). The peaks at 2.7 (a), 0.7 (b), and 0 (c) ppm are from the remaining organic fragments and can be assigned to the propyl chain $-OCH^a{}_2CH^b{}_2CH^c{}_3$. The deconvoluted intensities of these three peaks are approximately in the ratio 2:2:3 and they diminish simul-

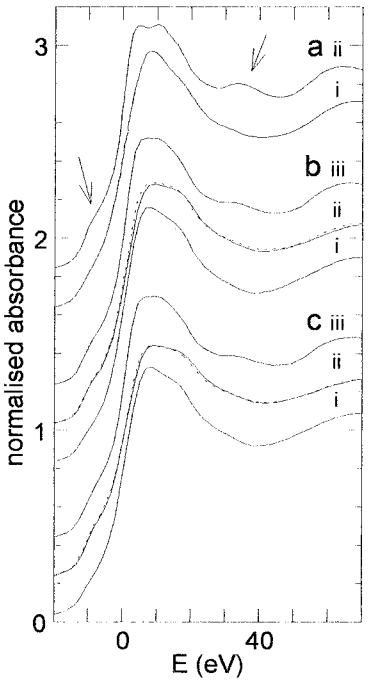

Figure 2. Zr K-edge XANES spectra of (a) reference compounds (i) m-ZrO_2 and (ii) t-ZrO_2. (Left and right arrows indicate p−d mixing and multiple scattering features, respectively.) XANES spectra are shown for the undoped ZrO_2 produced by the (b) sol−gel and (c) hydroxide-precipitation routes for samples (i) at room temperature immediately after manufacture (as-made), (ii) in situ at 340/320 °C immediately after reaching temperature and after 2 h (dashed lines), and (iii) at room temperature after 2 h at 500 °C. (Vertical offsets have been used for clarity.)

taneously as the organic groups are removed from the system. The 4.9 ppm resonance can then be directly attributed to OH. This peak has measurable intensity up to 500 °C, whereas the other peaks are lost after the sample is heated at 360 °C for 15 h. To exploit the quantitative advantage of NMR measurements, these ^{1}H MAS NMR spectra were integrated (spinning sidebands made a negligible contribution), and the intensity

Table 3. Summary of NMR Results on ^{17}O-Enriched Sol−Gel-Prepared Pure ZrO_2

	^{17}O NMR			
sample	δ_{iso} (ppm)	line width (Hz)	integrated intensity (%)	H content (mol/g)
as-made (20 °C)	405	1740	54	0.043 ± 0.001
	303	1860	46	
110 °C, 2 h	403	1960	56	0.026 ± 0.001
	308	1900	44	
220 °C, 2 h	406	1980	54	0.014 ± 0.001
	312	2180	46	
300 °C, 2 h	411	2520	60	0.009 ± 0.001
	320	2030	40	
360 °C, 2 h	403	2190	50	0.009 ± 0.001
	317	2260	50	
360 °C, 15 h	411	2100	43	0.007 ± 0.001
	374	1130	17	
	321	2250	40	
380 °C, 2 h	417[a]	200	2	0.005 ± 0.001
	377	700	87	
	328	500	11	
500 °C, 2 h	403	690	20	0.004 ± 0.001
	377	770	60	
	326	690	20	
700 °C, 2 h	400	520	44	<0.001
	374	390	13	
	322	390	43	

[a] Peak poorly defined subject to large errors. Typical errors in the parameters were ±1 ppm in δ_{iso}; ±50 and ± 20 Hz in $\Delta\nu$ prior to and after crystallization, respectively; and ±5% in the intensity. In estimating the ^{1}H content after the sample is heated to 700 °C, the signal is comparable with the error.

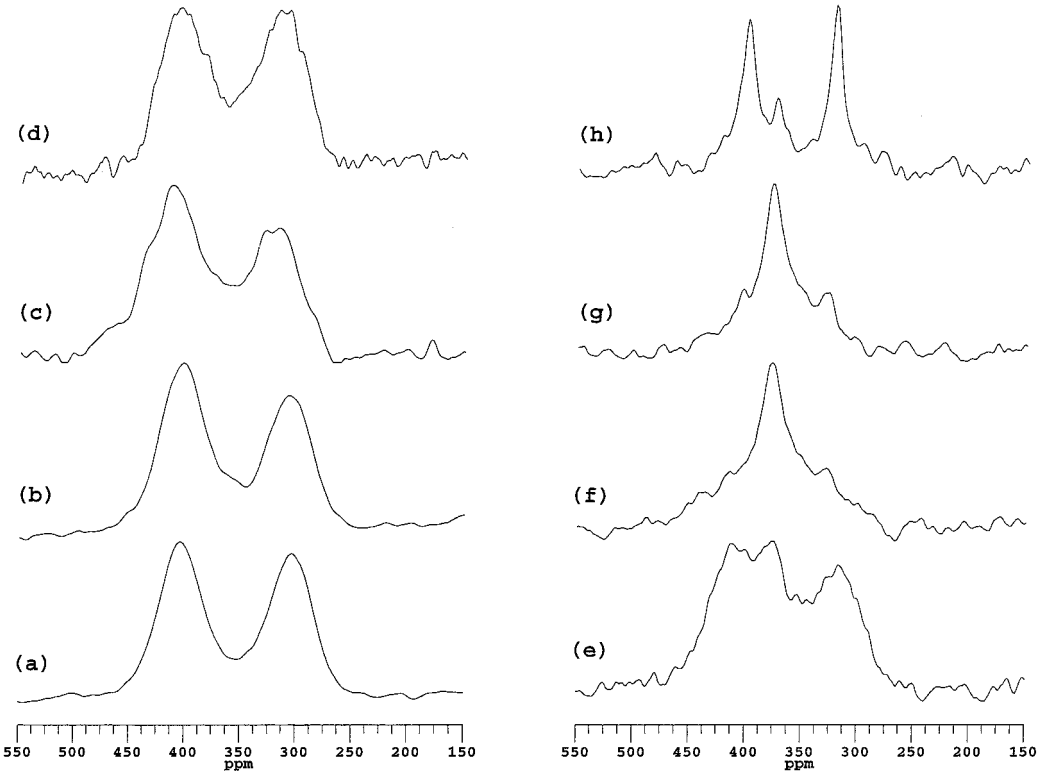

Figure 3. ^{17}O MAS NMR spectra of sol−gel-prepared undoped ZrO_2 undergoing the successive heat treatments given in Table 3 for the samples (a) as-made and after treatment at (b) 220 °C, (c) 300 °C, (d) 360 °C, (e) 360 °C (for a further 15 h), (f) 380 °C, (g) 500 °C, and (h) 700 °C.

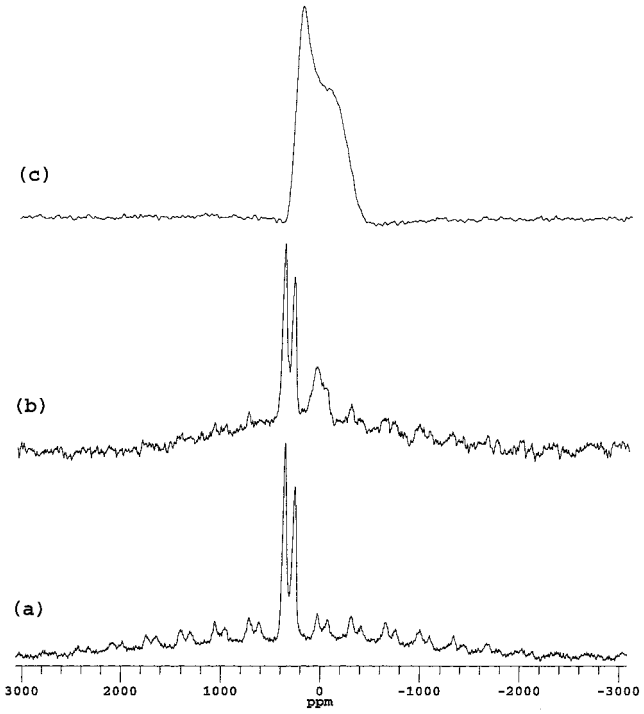

Figure 4. ^{17}O NMR spectra over a wider frequency range of (a) the as-made sample using direct acquisition under MAS and the sample after treatment for 2 h at 110 °C using (b) direct acquisition under MAS and (c) $^{1}H-^{17}O$ CP static measurements.

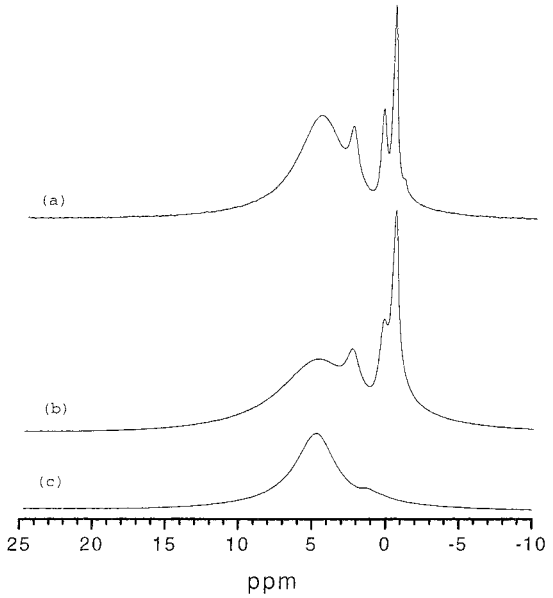

Figure 5. ^{1}H MAS NMR spectra of the undoped sol−gel-prepared ZrO_2 sample undergoing the successive heat treatments given in Table 3 for the sample (a) as-made and after treatment (b) at 220 °C and (c) for 15 h at 360 °C.

associated with OH was determined by fitting the 4.9 ppm peak to a Lorentzian line shape (Table 3). The H content associated with OH decreases monotonically with increasing heat treatment, with a small step obvious at the crystallization point but still with significant proton content (Figure 6).

In $^{1}H-^{13}C$ CP MAS NMR spectra, three weak, sharp peaks were detected at 64.9, 25.3 and 9.5 ppm (Figure 7). There is a broader and even weaker peak at ~165 ppm. On heating, the peaks decrease in intensity, with

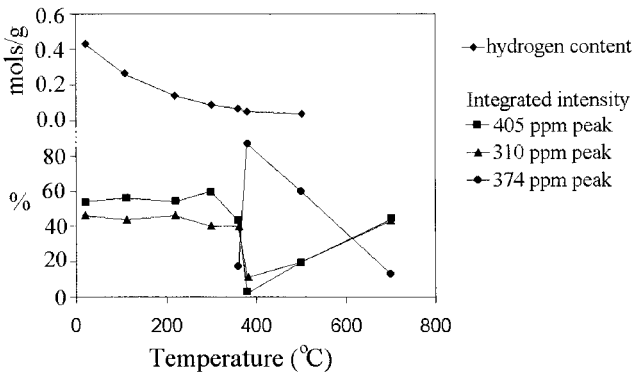

Figure 6. Summary of the NMR data on the proton content determined from ^{1}H NMR measurements and the integrated peak intensities for the three main resonances in the ^{17}O MAS NMR spectra.

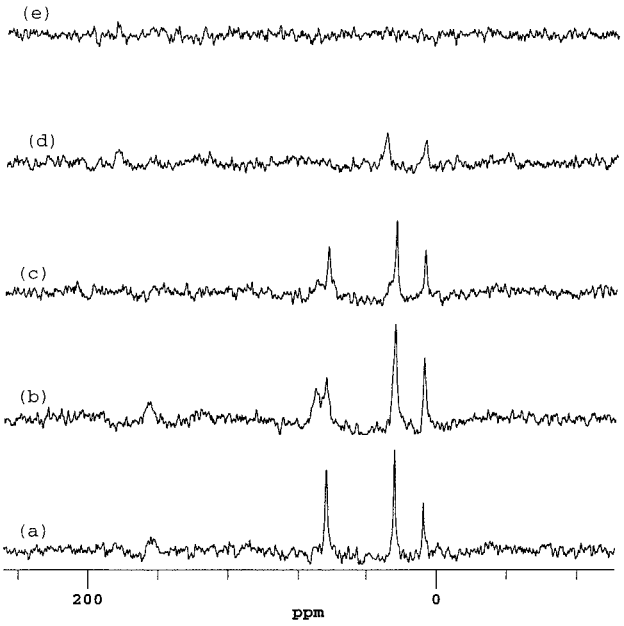

Figure 7. ^{13}C CP MAS NMR spectra of the undoped sol−gel-prepared sample undergoing the successive heat treatments given in Table 3 for the sample (a) as-made and after treatment at (b)110 °C, (c) 220 °C, (d) 300 °C, and (e) 360 °C.

the ~65 ppm peak broadening, and after 15 h at 360 °C, the CP carbon signal is entirely absent (Figure 7e). The three sharp resonances can be assigned to the propyl chain as 64.9 (a), 25.3 (b), and 9.5 (c) ppm, and the protons on these groups are the major source of the CP signal because of their spatial proximity. The carbon content is rapidly lost compared to the OH content and is completely removed prior to crystallization. The apparent differential loss of the 64.9 ppm resonance results from increased broadening of this peak compared to the other two because of the much greater chemical shift dispersion at this site, as it is directly attached to the zirconia network. The weak peak at ~165 ppm could be due to some minor carbonate[43] formation.

4. Discussion

EXAFS measurements of the amorphous doped and undoped samples prepared via both routes below ~360

(43) Papenguth, H. W.; Kirkpatrick, R. J.; Montez, B; Sandberg, P. A. *Am. Mineral.* **1989**, *74*, 1152.

°C are best fitted to a nearest-neighbor oxygen coordination number of 7 and a weak Zr−Zr correlation with 4 neighbors. The nearest-neighbor oxygen coordination number of 7 is certainly suggestive of having a local structure closer to monoclinic than tetragonal. In the EXAFS results, the clearest difference between the cubic and monoclinic structures is in the Zr−Zr correlation(s) (Table 2), and the Zr−Zr distances determined here in the amorphous samples are more similar to those in the monoclinic samples. The XANES results also suggest that the initial gel has a monoclinic-like structure. On crystallization, the room-temperature stable crystalline phase in all samples is tetragonal (t), with the EXAFS data showing a splitting of the Zr−O correlation and an increase in the intensity of the Zr−Zr correlation to a level close to that expected for t-ZrO_2, although the DW factor is significantly increased compared to bulk phases. The fitting of the second shell is statistically significant, but the higher DW factor shows that it is much less tightly defined than the inner shell. It is a general observation for the EXAFS spectra of nanocrystalline oxides that either the coordination number decreases or the DW factor increases or both compared to bulk samples, reflecting the increased disorder in nanoparticles.[44] At the point of crystallization, the XANES spectra are also consistent with the tetragonal structure.

As the particle size increases, the Zr−Zr correlation becomes better defined, which is reflected in the decrease of its DW factor. Then, on further heating, as the particles grow in undoped ZrO_2 samples heated to ≥700 °C, a monoclinic structure is observed at room temperature. The monoclinic-like structure of the samples is also reflected in the EXAFS spectra being better simulated by monoclinic parameters for both Zr−O and Zr−Zr correlations. Room-temperature XRD of the pure sol−gel sample heated to 700 °C shows a mixture of mostly m-ZrO_2 with some t-ZrO_2. Doped samples, even those samples heated to 1000 °C, when cooled back down to room temperature, remain as t-ZrO_2.

Both dopants and crystallite size effect the phases present, and the data presented here agrees with the results of other recent studies.[45,46] The data circumstantially suggest the role of the crystallite size in undoped samples in controlling the phase transformation. However, these systems are complex, and it is not really possible to distinguish between (i) the transformation being surface-free-energy-driven, and hence being solely dependent on crystallite size, and (ii) the effect of embryonic nuclei that transform domains when they reach a critical size. The role of defects, in this case hydroxyl groups, can also play a crucial role in stabilizing the tetragonal phase at room temperature. The EXAFS and XANES data suggest that the amorphous precursor structure is monoclinic-like rather than tetragonal and very similar for all samples. This closely agrees with wide-angle X-ray scattering experiments, which found that the radial correlation function of amorphous zirconia xerogels and aerogels bore much more resemblance to m- than t-ZrO_2.[47] It also agrees with EXAFS data from zirconium hydroxide, which indicated a structure similar to m-ZrO_2.[48]

The suggested structure must also be consistent with the NMR data. To better appreciate the information in the ^{17}O MAS NMR spectra, the sources of the line broadening must be elucidated. In amorphous samples, the local structure (as also reflected in the Zr−O correlation of the EXAFS data) is little changed from that in crystalline compounds, so that the electric field gradient will not change significantly. ^{17}O NMR work on TiO_2[24] and La_2O_3[27] gels showed that the line widths scaled directly with the applied magnetic field, indicating that the line width is largely determined by chemical shift dispersion and that second-order electric quadrupole effects are small. Hence, narrower lines indicate a reduced range of environments through a smaller chemical shift dispersion. An estimate of the quadrupole contribution to the center band MAS line width can be made by noting that the spinning sidebands span a range of ±100 kHz (Figure 5a), which, for a spin-$^5/_2$ nucleus, corresponds to $3C_Q/5$. This gives $C_Q \approx 167$ kHz which will produce second-order quadrupole broadening in the center band of <5 Hz, i.e., quadrupole effects can be neglected for the center bands of Zr−O−Zr fragments.

The two ^{17}O resonances at 405 and 303 ppm are close to the positions of bulk crystalline m-ZrO_2 at 404 and 322 ppm.[49] Nevertheless, on the basis of the isotropic chemical shift (which is very close to the peak position, as C_Q is so small that second-order isotropic shifts are ≤0.1 ppm), the local structure is monoclinic-like, as the gel has both OZr_3 (405 ppm) and OZr_4 (303 ppm) environments in approximately equal proportions. NMR spectra provide a clear distinction from c-ZrO_2, which has a single ^{17}O NMR peak at 355 ppm, and thus can definitely be excluded in the precursor gel. As the amorphous gel is heated, these two oxygen environments remain, although there is an obvious increase in line width. This indicates that the chemical shift dispersion increases, reflecting an increase in the range of local environments and, hence, the degree of disorder in the gel. There is also an increase in the isotropic chemical shift of the peaks, especially the OZr_4 peak, which moves from 303 to 321 ppm as the gel starts to crystallize. In HfO_2, which is chemically very similar to ZrO_2, the OHf_4 peak shifts from 245 ppm in the as-prepared gel to 258 ppm in the amorphous gel immediately prior to crystallization.[26] The chemical shift is determined by the electron density in the bonds around a nuclear site which can be correlated to the coordination number, π-bond order, and bond length. Solution-state ^{17}O NMR studies of polyoxometalate complexes have shown that the ^{17}O shift in molybdates and vanadates can be correlated to the shortest O−M distance.[50] Such a correlation is likely to apply generally to O−M bonds, simply scaling for different metals. Hence, an increase in the shift by ∼20 ppm corresponds to a decrease in the mean shortest bond length at the

(44) Nitsche, R.; Winterer, M.; Croft, M.; Hahn, H. *Nucl. Instrum. Methods Phys. Res. B* **1995**, *97*, 127.
(45) Lin, J.-D.; Dih, J. G. *J. Am. Ceram. Soc.* **1998**, *81*, 853.
(46) Stichert, W.; Schuth, F. *Chem. Mater.* **1998**, *10*, 2020.
(47) Zeng, Y. W.; Fagherazzi, G.; Pinna, F.; Polizzi, S.; Riello, P.; Signoretti, M. *J. Non-Cryst. Solids* **1993**, *155*, 259.
(48) Turrillas, X.; Barnes, P.; Dent, A. J.; Jones, S. L.; Norman, C. J. *J. Mater. Chem.* **1993**, *3*, 583.
(49) Bastow, T. J.; Stuart, S. N. *Chem. Phys.* **1990**, *143*, 459.
(50) Howarth, O. W. *Polyoxometalates*; Pope, M. T., Mueller, A., Eds.; Kluwer Academic: Dordrecht, The Netherlands, 1994; p 167.

OZr_4 site, which is consistent with an approach to a precursor local environment that becomes tetragonal on crystallization. Conversion of Zr−OH to Zr−O−Zr could also result in a decrease of the Zr−O distance.

Then, *after* crystallization has occurred, there is an additional ^{17}O NMR peak at 374 ppm that corresponds to OZr_4 in t-ZrO_2. The NMR data reflect all of the oxygen environments present and show that, although crystalline t-ZrO_2 is forming at the point of crystallization, a lot of the oxygen is still present as disordered ZrO_2. After further heating, the tetragonal content increases markedly, but at no time is there complete elimination of disordered ZrO_2, which could easily be missed by other techniques. This result is consistent with models of nanocrystalline solids in which there is always a significant amount of disordered interfacial material. In samples heated to higher temperatures, monoclinic structures form in the room-temperature samples with peaks at ∼400 and 322 ppm in the expected 1:1 ratio.

^1H NMR results show that, even at crystallization, it is not correct to describe the sample composition as ZrO_2. Assuming $ZrO_x(OH)_y$ (this ignores the OCH_2CH_2-CH_3 fragments, which ^1H NMR data show are present up to 300 °C), ^1H NMR data suggest that, after being heated to 300 °C, the sample's composition is $ZrO_{1.42}$-$(OH)_{1.16}$, and at 500 °C, well above the crystallization temperature, it is still $ZrO_{1.76}(OH)_{0.48}$. It should be stressed that this OH content is *not* related to the usual surface hydroxylation of such an oxide on exposure to the atmosphere (care was taken to minimize this contact), as after the heat treatment at 700 °C, the OH content is reduced below the accuracy of the measurement. Hence, most of the OH groups recorded at ≤500 °C must be structural units *within* the sample and not simply surface OH, so they could be within the nanocrystalline phase or part of a separate amorphous phase.

The NMR and Zr K-edge EXAFS and XANES results taken together unambiguously indicate that the short-range structure of the amorphous gel is monoclinic-like. All of these data suggests that, as the sample is heated, some minor modification of the structure occurs, but in the amorphous state, it remains monoclinic-like. Crystallization results in a change of structure to give tetragonal crystalline nanoparticles, but a large fraction of the sample remains amorphous. ^{17}O NMR results suggest that this amorphous/disordered content is monoclinic-like. At the point of crystallization, the Zr−K edge EXAFS and XANES data, using a single set of parameters, are better described by those for the tetragonal phase. This is somewhat surprising, as the short-range nature of the X-ray absorption techniques makes them sensitive to short-range structure so they should readily detect m-ZrO_2 even if it is disordered. It should be re-emphasized here that no simulations were tried based on two components because the relatively broad shells meant that such simulations would involve significant uncertainties as to their uniqueness. The X-ray absorption techniques scatter from the entire sample, giving an average for the complete sample and so should reflect both components. The presence of an amorphous component in the sample should decrease the intensity of the second (and further) shells. The Debye−Waller factors are increased relative to those of the model crystalline solids but not to the extent expected given the amount of monoclinic structure indicated by the ^{17}O NMR data. The most likely cause of this apparent discrepancy is that the EXAFS and NMR measurements were not carried on identical samples. Both are nominally "at the point" of crystallization, but at the phase transition, the amorphous/crystalline ratio is extremely sensitive to the thermal history, which influences the kinetics (as opposed to thermodynamic equilibrium). Hence, it appears that the NMR sample was heated very close to this point and that conversion was progressing very slowly so that only small amounts of t-ZrO_2 (as confirmed by the laboratory XRD measurements) formed. The EXAFS sample might have been at a slightly higher temperature, where crystalline t-ZrO_2 was more rapidly produced as the dominant phase. Away from this transition point, where the phases observed are much less critically dependent on the heat treatment, the NMR and X-ray absorption results are in very good agreement. All techniques do agree that the crystalline material that initially forms is tetragonal. Then, as the heat treatment time or temperature (up to ∼500 °C) is increased, the amount of t-ZrO_2 in the sample, even after it is cooled back to room temperature, increases. After heat treatment at higher temperatures, in pure ZrO_2 samples cooled back to room temperature, the formation of m-ZrO_2 occurs. In samples doped with 8% yttrium, t-ZrO_2 is stabilized in the samples cooled back to room temperature.

5. Summary and Conclusions

In forming zirconia from the sol−gel or hydroxide-precipitation routes, the reaction has been crudely represented as $[Zr_4O_{(8-x)}(OH)_{2x}] \rightarrow ZrO_2$ (amorphous) → ZrO_2 (t, crystalline). The details of these structural changes are undoubtedly complex, particularly those of the amorphous hydrous zirconia intermediate. Turrillas et al. proposed a three-stage calcination process as hydroxyl liberation and cross-linking occur.[9] The data presented here can be interpreted consistently within this framework but place additional constraints on the structure in that they clearly show that the hydroxyl content remains significant even after crystallization has occurred. Although there might be OH-free domains of t-ZrO_2, the sample still has many OHs, probably in residual amorphous regions. This work agrees with the diffraction work of Zeng et al.[47,51] in that the amorphous samples are distinctly monoclinic-like and, after the initial crystallization, the structure is a complex mixture of monoclinic-like and tetragonal domains. Dehydroxylation is not complete *prior* to crystallization, and there is no evidence from these data that the structure of the amorphous gel becomes more tetragonal-like, as has recently been suggested on the basis of X-ray radial distribution functions[52] and X-ray diffraction data.[53] In trying to understand the structural development of complex systems that involve amorphous/disordered intermediates it is important to accumulate comprehensive experimental data sets. In systems where

(51) Zeng, P. W., Fagherazzi, G.; Polizzi, S. *J. Mater. Sci.* **1995**, *30*, 2153.
(52) Stachs, O.; Gerber, T.; Petkov, V. *J. Non-Cryst. Solids* **1997**, *210*, 14.
(53) Gomez, R.; Lopez, T.; Bokhimi, X.; Munoz, E.; Novaro, O. *J. Sol−Gel Sci. Technol.* **1998**, *11*, 309.

amorphous components are significant, complementary atomic-scale information greatly strengthens any models and reduces the chances of ambiguity. The suggested reaction scheme for a sample with no doping is of the initial hydroxide becoming an amorphous oxide containing hydroxyls. With heating, some of these hydroxyls are lost, resulting in the formation of a mixture with more-ordered tetragonal and less-ordered monoclinic components and with the eventual crystalline product being monoclinic. The process can be represented as $Zr_4O_{(8-x)}(OH)_{2x} \rightarrow ZrO_{(2-y/2)}$(amorphous)$(OH)_y \rightarrow ZrO_{(2-z/2)}$(t,crystalline, m-like disordered)$(OH)_z \rightarrow ZrO_2$(m,crystalline). This system is extremely complex, but the extensive experimental data presented here for ZrO_2 produced via two routes has provided new information on the details of the structural development and could be important for tailoring nanocrystalline ZrO_2.

Acknowledgment. The EPSRC is thanked for its support of work on nanocrystalline oxides through Grant GR/K74876 and for the support of NMR equipment through JREI awards. Drs. A. Dent, F. Mosselmans, and I. Harvey are thanked for their help in using Station 9.3 at the Daresbury SRS. MGT thanks UKC for partial support during this study.

CM001152W